

# Origins of fractality in the growth of complex networks

Chaoming Song<sup>1</sup>, Shlomo Havlin<sup>2</sup>, and Hernán A. Makse<sup>1</sup>

<sup>1</sup> *Levich Institute and Physics Department,  
City College of New York, New York, NY 10031, US*

<sup>2</sup> *Minerva Center and Department of Physics,  
Bar-Ilan University, Ramat Gan 52900, Israel*

(Dated: October 6, 2018)

## Abstract

Complex networks from such different fields as biology, technology or sociology share similar organization principles. The possibility of a unique growth mechanism for a variety of complex networks in different fields such as biology, technology or sociology is of interest, as it promises to uncover the universal origins of collective behavior. The emergence of self-similarity in complex networks raises the fundamental question of the growth process according to which these structures evolve. Here, we use the concept of renormalization as a mechanism for the growth of fractal and non-fractal modular networks. We show that the key principle that gives rise to the fractal architecture of networks is a strong effective “repulsion” (disassortativity) between the most connected nodes (hubs) on all length scales, rendering them very dispersed. More importantly, we show that a robust network comprised of functional modules, such as a cellular network, necessitates a fractal topology, suggestive of an evolutionary drive for their existence.

An important result in statistical physics was the generation of fractal geometries by Mandelbrot [1, 2], the structures of which look the same on all length scales. Their importance stem from the fact that these structures were recognized in numerous examples in Nature, from snowflakes and trees to phase transitions in critical phenomena [2, 3]. While these fascinating patterns are only geometric, new forms of topological fractality have been observed in complex networks [4] where the links rely on interactions between the participants [5, 6]. Examples of topological fractal networks include the hyperlinks in the WWW, physical interactions in protein interaction networks or biochemical reactions in metabolism [4, 7]. Other complex networks such as the Internet do not share the topological fractal property.

These fractal complex networks are characterized by the small-world property (as given by the logarithmic dependence of the average distance with the number of nodes) brought about by the “short-cuts” in the network [8], a very wide (power-law or “scale-free” [9]) distribution of connections, and a modular hierarchical structure [10, 11, 12, 13]. However, the fractal sets of Mandelbrot do not exhibit these features. While in our previous work [4], we discovered the fractal nature of organization in many real networks the question remained how these networks have evolved in time. We therefore launch a study of growth mechanisms to understand the simultaneous emergence of fractality, modularity, as well as the small world effect, and the scale-free property in real world complex networks. Our results have important evolutionary implications. They highlight an evolutionary drive towards fractality, inspired by an increase in network robustness. Thus, a robust modular network requires a fractal topology. Furthermore, our analysis indicates that the fractal clusters can be identified with the functional modules in the case of the metabolic network of *E. coli*.

The “democratic” rule of the seminal Erdős-Rényi model [14] (where the nodes in the network are connected at random) was first invoked to explain the small world effect. It was then replaced by the “rich-get-richer” principle of preferential attachment [9] to explain the scale-free property; a discovery carrying important implications on network vulnerability [15, 16]. However these rules do not capture the fractal topologies found in diverse complex networks. We find that models of scale-free networks are not fractals (see Supplementary Materials Section I). Here, we demonstrate a new view of network dynamics where the growth takes place *multiplicatively* in a correlated self-similar modular fashion, in contrast

to the uncorrelated growth of models of preferential attachment [5, 9].

We formalize these ideas by borrowing the concept of “length-scale renormalization” from critical phenomena [3]. In this paper, we will show that the emergence of self-similar fractal networks, such as cellular ones, is due to the strong repulsion (disassortativity [17]) between the hubs at all length scales. In other words, the hubs prefer to grow by connections to less-connected nodes rather than to other hubs, an effect that can be viewed as an effective hub repulsion. In this new paradigm, the “rich” still get richer, although at the expense of the “poor”. In other words, the hubs grow by preferentially linking with less-connected nodes to generate a more robust fractal topology. In contrast, weakly anticorrelated or uncorrelated growth leads to non-fractal topologies such as the Internet.

**Growth mechanism.**— The renormalization scheme tiles a network of  $N$  nodes with  $N_B(\ell_B)$  boxes using the box-covering algorithm [4], as shown in Fig. 1a. The boxes contain nodes separated by a distance  $\ell_B$ , measured as the length of the shortest path between nodes. Each box is subsequently replaced by a node, and the process is repeated until the whole network is reduced to a single node. The way to distinguish between fractal and non-fractal networks is represented in their scaling properties as seen in Fig. 2a and 2b. Fractal networks can be characterized by the following scaling relations (Fig. 2a):

$$N_B(\ell_B)/N \sim \ell_B^{-d_B} \quad \text{and} \quad k_B(\ell_B)/k_{hub} \sim \ell_B^{-d_k}, \quad (1)$$

where  $k_{hub}$  and  $k_B(\ell_B)$  are the degree of the most connected node inside each box and that of each box respectively (Fig. 1a). Although both of them are partial variables, the ratio between them is a global quantity, depending only on the length scale  $\ell_B$ , as we showed in [4]. The two exponents  $d_B$  and  $d_k$  are the fractal dimension and the degree exponent of the boxes, respectively. While the term “fractal dimension” is usually reserved for geometrical self-similarity, here we relax the usage to include the topological self-similarity as well. For a non-fractal network like the Internet (Fig. 2b), we have  $d_B \rightarrow \infty$  and  $d_k \rightarrow \infty$ ; the scaling laws in Eq. (1) are replaced by exponential functions.

Based on the results leading to Eq. (1), we propose a network growth dynamics as the inverse of the renormalization procedure. Thus, the coarse-grained networks of smaller size are network structures appearing earlier in time, as exemplified in Fig. 1a. A present time network with  $\tilde{N}(t)$  nodes is tiled with  $N_B(\ell_B)$  boxes of size  $\ell_B$ . Each box represents a node in a previous time step, so that  $\tilde{N}(t-1) = N_B(\ell_B)$ . The maximum degree of the nodes

inside a box corresponds to the present time degree:  $\tilde{k}(t) = k_{hub}$ , which is renormalized such that  $\tilde{k}(t-1) = k_B(\ell_B)$ . The tilde over the quantities are needed in order to differentiate the dynamical quantities, such as the number of nodes as a function of time,  $\tilde{N}(t)$ , from the static quantities, such the number of nodes of the present network,  $N$ , or the number of nodes of the renormalized network,  $N_B$ . The renormalization procedure applies to many complex networks in Nature [4]. These includes fractal networks such as WWW, protein interaction networks of *E. coli*, the yeast [18] and human, and metabolic networks of 43 different organisms from the three domains of life, and some sociological networks. The renormalization scheme can be applied to non-fractal networks, such as the Internet, as well. Below we will show that the main difference between these two groups is in the connectivity correlation. We also provide empirical, analytical and modelling evidences supporting this theoretical framework based on the validity of exponents, scaling theory, and statistical properties of the connectivity correlation.

**Correlation.**— A question of importance to elucidate the selection rules governing the fractality of the network is to determine how the nodes in older networks are connected to those of the present day. The answer lies in the statistical property of correlation between the nodes and boxes within a network configuration. Studying the correlation profile in real networks similar to those considered in [17, 19, 20] provides initial hints to the above question. The correlation profile [19] compares the joint probability distribution,  $P(k_1, k_2)$ , of finding a node with  $k_1$  links connected to a node with  $k_2$  links with their random uncorrelated counterpart,  $P_r(k_1, k_2)$ , which is obtained by random swapping of the links, yet preserving the degree distribution. A plot of the ratio  $R(k_1, k_2) = P(k_1, k_2)/P_r(k_1, k_2)$  provides evidence of correlated topological structure that deviates from the random uncorrelated case.

At first glance, a qualitative classification based on the strength of the anticorrelation of different networks can be obtained by normalizing the ratio  $R(k_1, k_2)$  to that of a given network, for instance the WWW [21], (Supplementary Materials, Section II). Figure 2c and 2d show the correlation profiles of the cellular metabolic network of *E. coli* [22], which is known to be fractal, and the Internet at the router level [23], which has a non-fractal topology. The fractal network poses a higher degree of anticorrelation or disassortativity; nodes with a large degree tend to be connected with nodes of a small degree. On the other hand, the non-fractal Internet is less anticorrelated. Thus, fractal topologies seem to display a higher degree of hub repulsion in their structure than non-fractals. However, for this

property to be the hallmark of fractality, it is required that the anticorrelation appears not only in the original network (captured by the correlation profiles of Fig. 2c and Fig. 2d), but also in the renormalized networks at all length scales. We note that other measures of anticorrelation, such as the Pearson coefficient  $r$  of the degrees at the end of an edge [17], cannot capture the difference between fractal and non-fractal network. We find that  $r$  is not invariant under renormalization.

**Mathematical model.**— To quantitatively link the anticorrelation at all length scales to the emergence of fractality, we next develop a mathematical framework and demonstrate the mechanism for fractal network growth. In the case of modular networks, stemming from Eqs. (1), we require that

$$\begin{aligned}\tilde{N}(t) &= n\tilde{N}(t-1), \\ \tilde{k}(t) &= s\tilde{k}(t-1), \\ \tilde{L}(t) + L_0 &= a(\tilde{L}(t-1) + L_0),\end{aligned}\tag{2}$$

where  $n > 1$ ,  $s > 1$  and  $a > 1$  are time-independent constants and  $\tilde{L}(t)$  is the diameter of the network defined by the largest distance between nodes. The first equation is analogous to the multiplicative process naturally found in many population growth systems [24]. The second relation is analogous to the preferential attachment rule [9]. It gives rise to the scale-free probability distribution of finding a node with degree  $k$ ,  $P(k) \sim k^{-\gamma}$ . The third equation describes the growth of the diameter of the network and determines whether the network is small-world [8] and/or fractal. Here we introduce the characteristic size  $L_0$ , the importance of which lies in describing the non-fractal networks. Since every quantity increases by a factor of  $n$ ,  $s$  and  $a$ , we first derive (Supplementary Materials Section IV) the scaling exponents in terms of the microscopic parameters:  $d_B = \ln n / \ln a$ ,  $d_k = \ln s / \ln a$ . The exponent of the degree distribution satisfies  $\gamma = 1 + \ln n / \ln s$ . The dynamics represented by Eqs. (2) consequently leads to a modular structure where modules are represented by the boxes. While modularity has often been identified with the scaling of the clustering coefficient [11], here we propose an alternative definition of “modular network” as the one whose statistical properties remain invariant (in particular, an invariant degree distribution with the same exponent  $\gamma$ , see Supplementary Materials Section III) under renormalization.

In order to incorporate different growth modes in the dynamical Eqs. (2) we consider, without loss of generality, two modes of connectivity between boxes, whose relative frequen-

cies of occurrence are controlled by the probability  $e$  representing the hub-hub attraction. (i) Mode I with probability  $e$  (Fig. 1b): two boxes are connected through a direct link between their hubs leading to hub-hub attraction. (ii) Mode II with probability  $1 - e$  (Fig. 1c): two boxes are connected via non-hubs leading to hub-hub repulsion or anticorrelation. We will show that Mode I leads to non-fractal networks while Mode II leads to fractal networks. In practice, though Eqs. (2) are deterministic, we combine these two modes according to the probability  $e$ , which renders our model probabilistic.

Formally, for a node with  $\tilde{k}(t - 1)$  links at time  $t - 1$ , we define  $\tilde{n}_h(t)$  as the number of links which are connected to hubs in the next time step (see Fig. 1a). Then the probability  $e$  satisfies:

$$\tilde{n}_h(t) = e \tilde{k}(t - 1). \quad (3)$$

Using the analogy between time evolution and renormalization, we introduce the corresponding quantity,  $n_h(\ell_B)$ , and defines the ratio  $\mathcal{E}(\ell_B) \equiv n_h(\ell_B)/k_B(\ell_B)$ . The nonlinear relation between  $t$  and  $\ell_B$  leads to the  $\ell_B$  dependence on  $\mathcal{E}$  (see Supplementary Materials, Section IV). In the extreme case of strong hub attraction, where the hubs of the boxes are connected at all length scales, we have  $\mathcal{E}(\ell_B) \sim \text{constant}$ . On the other hand, hub repulsion leads to decreasing  $\mathcal{E}(\ell_B)$  with  $\ell_B$ . From scaling we obtain a new exponent  $d_e = -\ln e / \ln a$  characterizing the strength of the anticorrelation in a scale-invariant way:

$$\mathcal{E}(\ell_B) \sim \ell_B^{-d_e}. \quad (4)$$

Fig. 2e shows  $\mathcal{E}(\ell_B)$  for two real fractal and non-fractal networks: a map of the WWW domain (nd.edu) consisting of 352,728 web-sites [21] and a map of the Internet at the router level consisting of 284,771 nodes [23]. We find that for the fractal WWW,  $d_e = 1.5$ , indicating that it exhibits strong anticorrelation. On the other hand, the non-fractal Internet shows  $\mathcal{E}(\ell_B) \sim \text{constant}$ .

These results confirm that fractal networks, including the protein interaction network [25] (with  $d_e = 1.1$ ) and the metabolic network of *E. coli* [22] (with  $d_e = 4.5$ ), do have strong hub repulsion at all length scales and non-fractal networks have no or weak hub repulsion.

A general limitation when analyzing the scaling behavior of complex networks is the small range in which the scaling is valid. This is due to the small-world property that restricts the range of  $\ell_B$  in Fig. 2. As an attempt to circumvent this limitation, we offer not only the empirical determination of the exponents but also scaling theory and models

where the exponents can be further tested. We should also point out that large exponents (such as  $d_e = 4.5$  for *E. coli*) may not be distinguishable from exponential behavior (infinite exponent). In this case, however the large exponent  $d_e$  for *E. coli* agrees with our theoretical framework, since it corresponds to a network with large anticorrelation in the connectivity and the subsequent small fractal dimension. In terms of the model, this corresponds to the limit of  $e \rightarrow 0$ .

Next we show how the different growth modes reproduce the empirical findings. While each mode leads to the scale-free topology, they differ in their fractal and small-world properties. Mode I alone ( $e = 1$ ) exhibits the small-world effect, but is not fractal due to its strong hub-hub attraction (see Fig. 1b). On the other hand, Mode II alone ( $e = 0$ , Fig. 1c) gives rise to a fractal network. However, in this case, the anticorrelation is strong enough to push the hubs far apart, leading to the disintegration of the small-world. Full details of the implementation of Mode I and Mode II are given in the Supplementary Materials Section IV A and V.

These results suggest that the simultaneous appearance of both the small-world and fractal properties in scale-free networks is due to a combination of the growth modes. In general, the growth process is a stochastic combination of Mode I (with probability  $e$ ) and Mode II (with probability  $1 - e$ ). For the intermediate ( $0 < e < 1$ ), the model predicts finite fractal exponents  $d_B$  and  $d_k$  and also bears the small-world property due to the presence of Mode I. Such a fractal small-world and scale-free network is visualized in Fig. 3a for  $e = 0.8$ . Supporting evidences are given by (i) Fig. 3b, which shows that the model with  $e = 0.8$  is more anticorrelated than the  $e = 1$  model (Mode I), (ii) Fig. 3c, which shows the power law dependence of  $N_B$  on  $\ell_B$  for the fractal structure ( $e = 0.8$ ), and the exponential dependence of the non-fractal structure ( $e = 1$ ), and (iii) Fig. 3d showing that Mode I reproduces  $\mathcal{E}(\ell_B) \sim \text{constant}$  while the  $e = 0.8$  model gives  $\mathcal{E}(\ell_B) \sim \ell_B^{-d_e}$ , which is in agreement with the empirical findings of Fig. 2e on real networks (the exponent  $d_e = -\ln 0.8 / \ln 1.4 = 0.66$  is predicted by the analytical formula according to Supplementary Material IV). Furthermore, in the Supplementary Materials Section IV A we show that the predicted scale-free distribution is invariant under renormalization. Although simplistic, this minimal model clearly captures an essential property of networks: the relationship between anticorrelation and fractality (see Methods for more details). We have also considered the contribution of loops, which we find does not change the general conclusions of this study.

**Modularity.**— The scale-invariant properties naturally lead to the appearance of a hierarchy of self-similar nested communities or modules. In this novel point of view, boxes represent nested modules of different length scales. The importance of modular structures is stressed in biological networks, where questions of function and evolutionary importance are put to the test [10, 11, 12, 13]. The relevant question is whether the self-similar hierarchy of boxes encodes the information about the functional modules in biological networks. To answer this question we analyze the fractal metabolic network of *E. coli* [22] which has been previously studied using standard clustering algorithms [11]. Here we show that by repeatedly applying the renormalization we produce a tree with branches that are closely related to the biochemical annotation, such as carbohydrates, lipids, amino acid, etc [11]. We renormalize the network at a given box size and cluster the substrates which belong to the same box and repeat the procedure to generate the hierarchical tree shown in Fig. 4a. In Fig. 4b (the right-bottom scheme), we see a subnet of the original metabolic network with 14 nodes. They correspond to the bottommost layer of the hierarchical tree in the left. The box covering with  $\ell_B = 3$  indicates that this subnet contains four modules. The coarse-grained network is shown in the right-middle with 4 nodes: A, B, C and D. The next stage of renormalization combines these four nodes to one single node or class. Following this algorithm, we coarse-grain the network and classify the nodes at different levels. In Fig. 5a, we show this classification for the entire metabolic network. The different colors correspond to distinct functional modules, as we annotate in the bottom of the tree (carbohydrates, lipids, etc.). The clear division of biological functions in the hierarchical tree suggests that the metabolic network is organized in a self-similar way.

The main known biochemical classes of the substrates emerge naturally from the renormalization tree, indicating that the boxes capture the modular structure of the metabolic network of *E. coli*. The same analysis reproduces the modular structure of the protein interaction network of the yeast further suggesting the validity of our analysis [18].

**Robustness.**— Finally our results suggest the importance of self-similarity in the evolution of the topology of networks. Understanding the growth mechanism is of fundamental importance as it raises the question of its motivation in Nature. For instance, given that systems in biology are fractal, there could be an evolutionary drive for the creation of such networks. A parameter relevant to evolution is the robustness of the network, which can be compared between fractal and non-fractal networks.

Non-fractal scale-free networks, such as the Internet, are extremely vulnerable to targeted attacks on the hubs [15]. In such non-fractal topologies, the hubs are connected and form a central compact core (as seen in Fig. 2b), such that the removal of few largest hubs (those with the largest degree) has catastrophic consequences for the network [15, 26]. Here we show that the fractal property of networks significantly increases the robustness against targeted attacks since the hubs are more dispersed in the network (see Fig. 2a). Figure 4c shows a comparison of robustness between a fractal and non-fractal network. The comparison is done between model networks of the same  $\gamma = 2.8$ , the same number of nodes (74,000), the same number of links, the same amount of loops and the same clustering coefficient (see Supplementary Materials Section VI). Thus the difference in the robustness seen in this figure is attributed solely to the different degree of anticorrelation. We plot the relative size of the largest cluster,  $S$ , and the average size of the remaining isolated clusters,  $\langle s \rangle$ , after removing a fraction  $f$  of the largest hubs for both networks [15]. While both networks collapse at a finite fraction  $f_c$ , evidenced by the decrease of  $S$  toward zero and the peak in  $\langle s \rangle$ , the fractal network has a significantly larger threshold ( $f_c \approx 0.09$ ) compared to the non-fractal threshold ( $f_c \approx 0.02$ ) suggesting a significantly higher robustness of the fractal modular networks to failure of the highly connected nodes. This could explain why evolutionary constraints on biological networks have led to fractal architectures. It is important to note that the comparison in Fig. 4c is between two networks which preserve the modularity. Our results should be understood as follows: given that a network has a modular structure, then the most robust network is the one with fractal topology. There are other ways to increase robustness by, for instance, fully connecting the hubs in a central core [29], but this arrangement does not preserve the modularity.

**Summary.**— We find that the statistical properties of many real networks are well consistent with the predictions of the proposed multiplicative model. Networks that can be captured by our theoretical framework include fractal networks (WWW, protein interactions, metabolic networks and some collaboration networks) and the non-fractal networks such as the Internet. The validity of the proposed framework is supported by the predicted scaling exponents ( $d_B$ ,  $d_k$ ,  $d_e$ ) in many real networks as well as the general properties of the connectivity distribution captured by  $P(k_1, k_2)$  and the scaling relationships predicted by the multiplicative growth process of our model. Our results demonstrate that nodes are organized around dispersed hubs in self-similar nested modules [13] characterized by

different functionalities. These then compartmentalize the hubs [19], and protect them from a failure at the system level [26]. Hence, these modules function relatively autonomously so that a failure in one module cannot propagate easily to the next. This may provide a significantly higher protection against intentional attacks reducing the high vulnerability—the Achilles' heel— of non-fractal scale-free networks.

## METHODS

**Details of the Mode I and Mode II of growth in the minimal model.**— Mode I: To each node with degree  $\tilde{k}(t-1)$  at time  $t-1$ ,  $m\tilde{k}(t-1)$  offspring nodes are attached at the next time step ( $m=2$  in the example of Fig. 1b). As a result we obtain a scale-free non-fractal network:  $N_B(l_B)/N \sim \exp(-\frac{\ln n}{2}l_B)$  and  $k_B(l_B)/k_{hub} \sim \exp(-\frac{\ln s}{2}l_B)$ , implying that both exponents  $d_B$  and  $d_k$  are infinite (since  $a \rightarrow 1$  then  $d_B = \ln n / \ln a \rightarrow \infty$  and  $d_k = \ln s / \ln a \rightarrow \infty$ ). This is a direct consequence of the linear growth of the diameter  $\tilde{L}(t)$ . Moreover, the additive growth in the diameter with time implies that the network is small-world. This mode is similar to a class of models called pseudo-fractals [27, 28]. Mode II: It gives rise to a fractal topology but with a breakdown of the small-world property. The diameter increases multiplicatively leading to an exponential growth with time, and consequently to a fractal topology with finite  $d_B$  and  $d_k$ .

FIG. 1. Self-similar dynamical evolution of networks. (a) The dynamical growth process can be seen as the inverse renormalization procedure with all the properties of the network being invariant under time evolution. In this example  $\tilde{N}(t) = 16$  nodes are renormalized with  $N_B(\ell_B) = 4$  boxes of size  $\ell_B = 3$ . (b) Analysis of Mode I, only: the boxes are connected directly leading to strong hub-hub attraction or assortativity. This mode produces a scale-free, small-world network but without the fractal topology. (c) Mode II alone produces a scale-free with a fractal topology but not the small-world effect. Here the boxes are connected via non-hubs leading to hub-hub repulsion or disassortativity.

FIG. 2. Empirical results on real complex networks. (a) Schematics showing that fractal networks are characterized by a power law dependence between  $N_B$  and  $\ell_B$  while (b) non-fractal networks are characterized by an exponential dependence. (c) Plot of the correlation profile of the fractal metabolic network of *E. coli*,  $R_{E.coli}(k_1, k_2)/R_{WWW}(k_1, k_2)$ , and (d) the non-fractal Internet  $R_{Int}(k_1, k_2)/R_{WWW}(k_1, k_2)$ , compared with the profile of the WWW in search of a signature of fractality. (e) Scaling of  $\mathcal{E}(\ell_B)$  as defined in Eq. (4) for the fractal topology of the WWW with  $d_e = 1.5$ , and the non-fractal topology of the Internet showing that fractal topologies are strongly anticorrelated at all length scales. In order to calculate  $\mathcal{E}$  (and in all the calculations in this study) we tile the network by first identifying the nodes which are the center of the boxes with the largest mass and sequentially centering the boxes around these nodes.

FIG. 3. Predictions of the renormalization growth mechanism of complex networks. (a) Resulting topology predicted by the minimal model for  $e = 0.8$ ,  $n = 5$ ,  $a = 1.4$ ,  $s = 3$  and  $m = 2$ . The colors of the nodes show the modular structure with each color representing a different box. We also include loops in the structure as discussed in the Supplementary Materials, Section VI. (b) Ratio  $R_{e=1}(k_1, k_2)/R_{e=0.8}(k_1, k_2)$  to compare the hub-hub correlation emerging from the model networks generated with  $e = 1$  and  $e = 0.8$ , respectively. (c) Plot of  $N_B$  versus  $\ell_B$  showing that Mode I is non-fractal (exponential decay) and  $e = 0.8$  is fractal (power-law decay) according to (b) and in agreement with the empirical results of Fig. 2. (d) Scaling of  $\mathcal{E}(\ell_B)$  reproducing the behavior of fractal networks for  $e = 0.8$  and non-fractal networks Mode I,  $e = 1$ , as found empirically in Fig. 2e.

FIG. 4. Practical implications of the renormalization growth approach and fractality. (a) Renormalization tree of the metabolic network of *E. coli* leading to the appearance of the functional modules. The colors of the nodes and branches in the tree denote the main

biochemical classes as: carbohydrates, lipids, proteins, peptides and aminoacids, nucleotides and nucleic acids, and coenzymes and prosthetic groups biosynthesis (grey). (b) Details of the construction of three levels of the renormalization tree for  $\ell_B = 3$  for 14 metabolites in the carbohydrate biosynthesis class as shown in the shaded area in (a). (c) Vulnerability under intentional attack of a non-fractal network generated by Mode I ( $e = 1$ ) and a fractal network generated by Mode II ( $e = 0$ ). The plot shows the relative size of the largest cluster,  $S$ , and the average size of the remaining isolated clusters,  $\langle s \rangle$  as a function of the removal fraction  $f$  of the largest hubs for both networks.

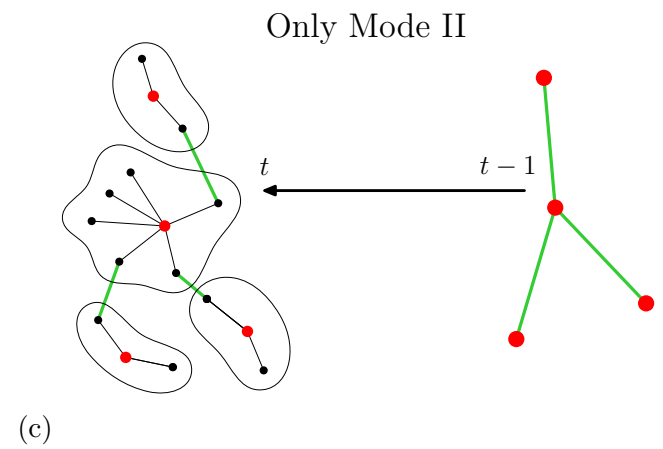
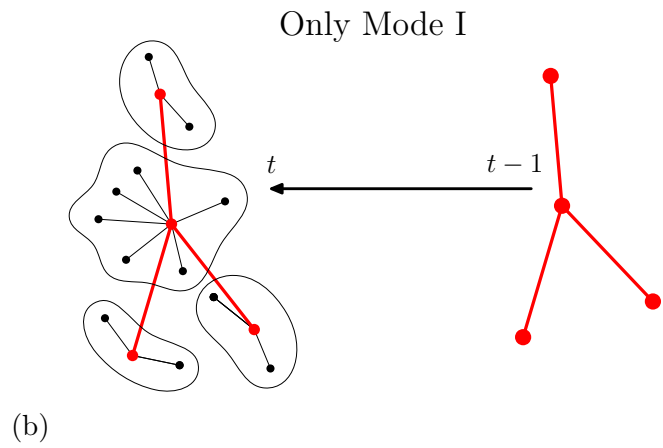
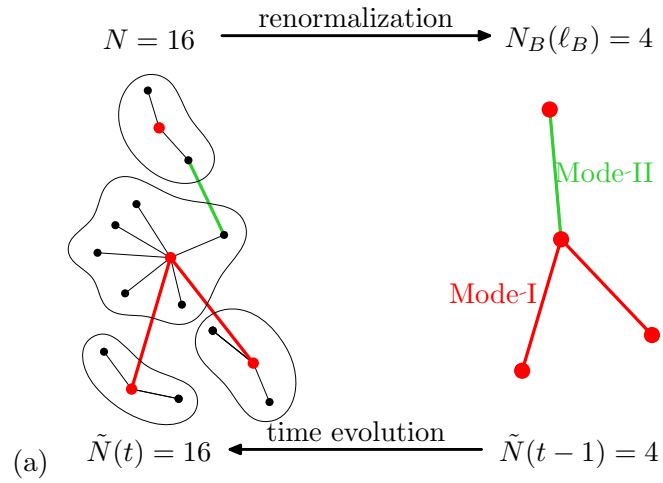


FIG. 1:

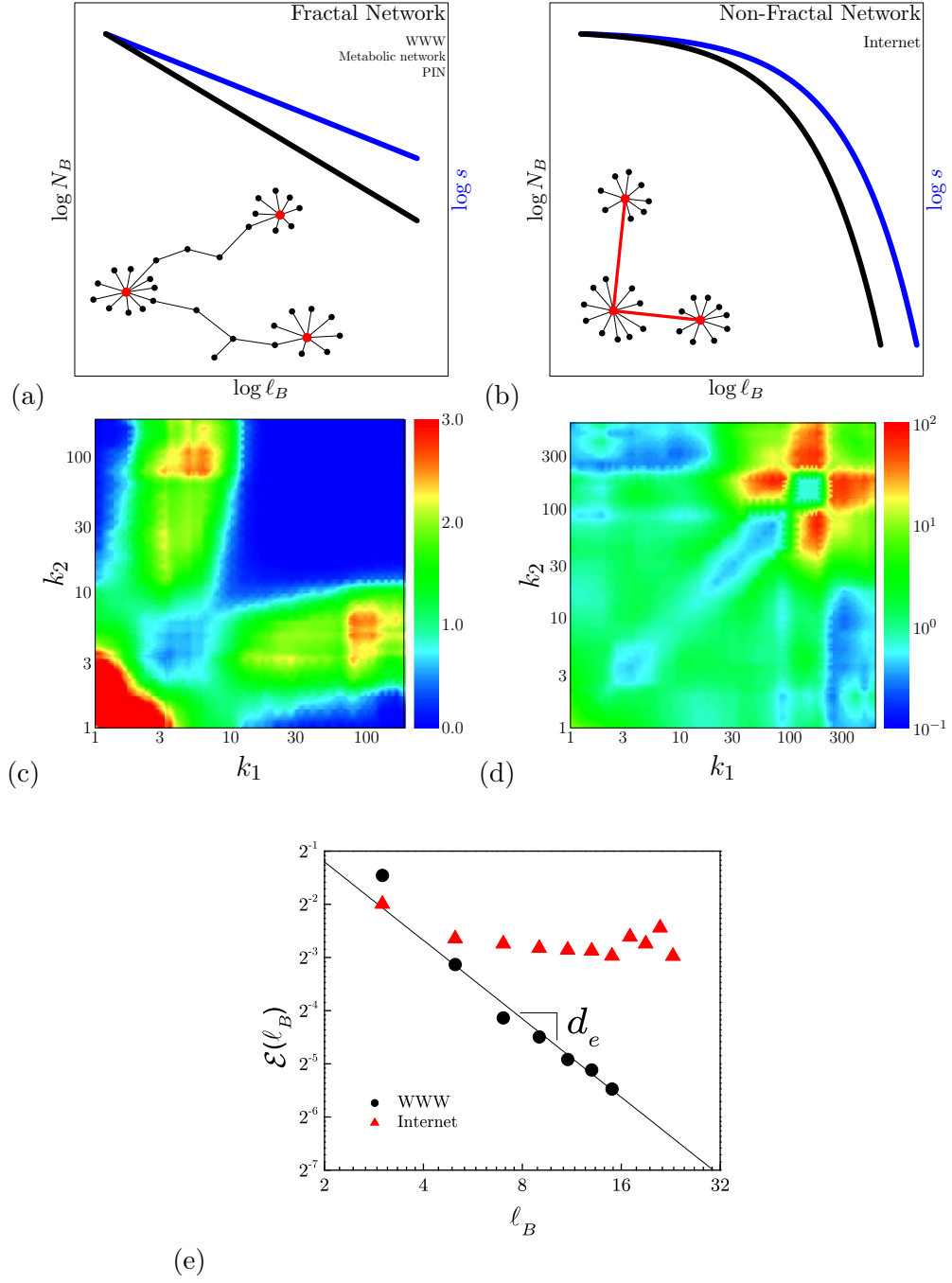


FIG. 2:

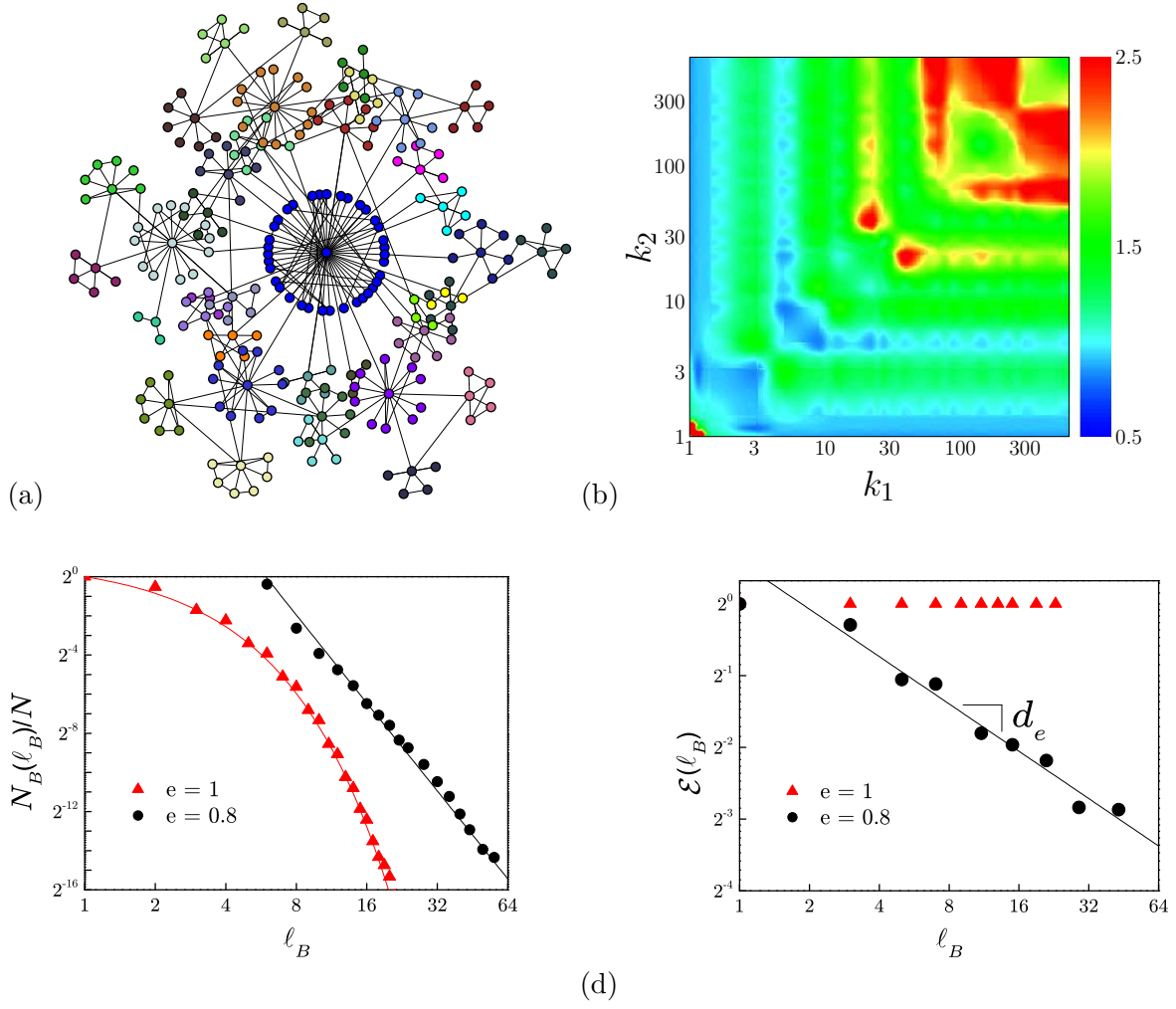


FIG. 3:

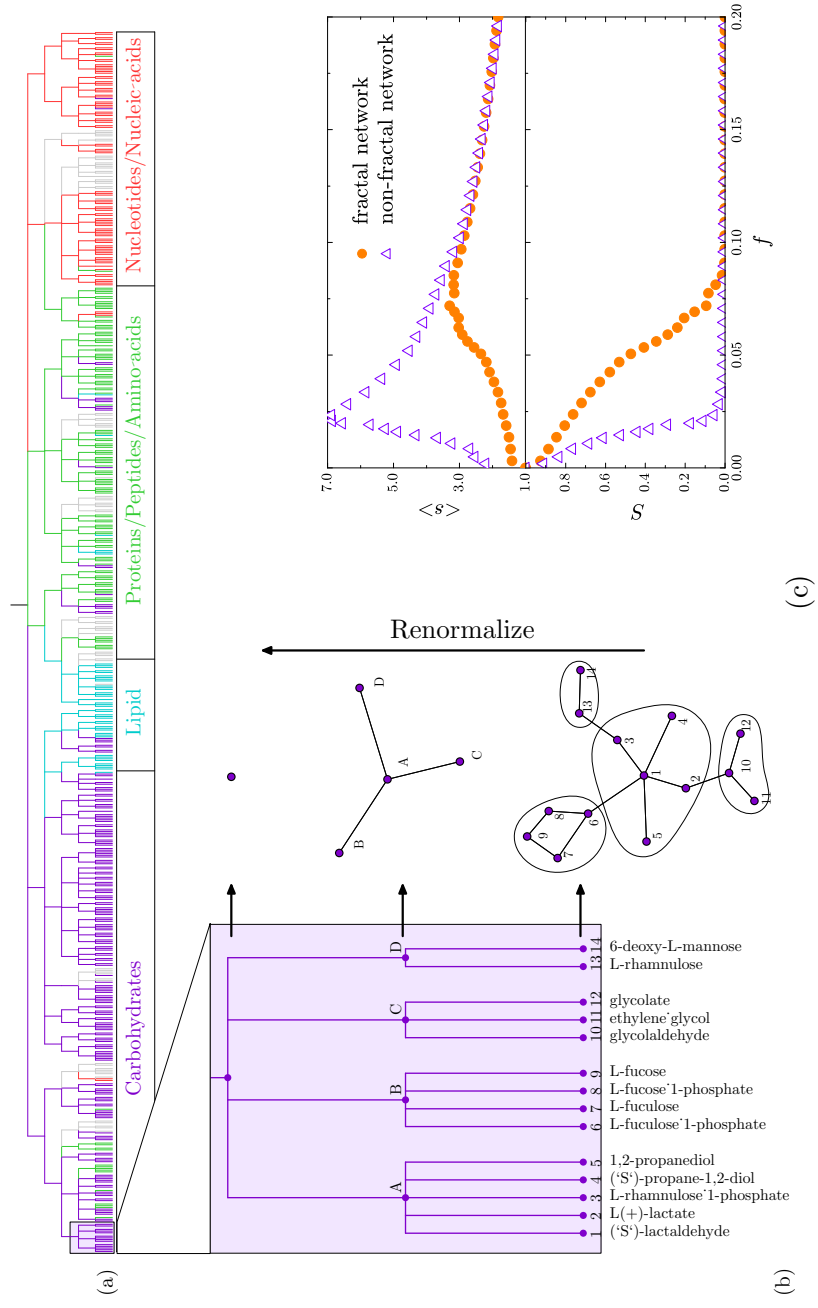


FIG. 4:

- 
- [1] Mandelbrot, B. B. *The Fractal Geometry of Nature* (Freeman Co., San Francisco, 1982).
- [2] Vicsek, T. *Fractal Growth Phenomena*, 2nd ed., Part IV (World Scientific, Singapore, 1992).
- [3] Stanley, H. E. *Introduction to Phase Transitions and Critical Phenomena* (Oxford University Press, Oxford, 1971).
- [4] Song, C., Havlin, S., Makse, H. A. Self-similarity of complex networks. *Nature* **433**, 392-395 (2005).
- [5] Albert, R., Barabási, A.-L. Statistical mechanics of complex networks. *Rev. Mod. Phys.* **74**, 47-97 (2002).
- [6] Pastor-Satorras, R., Vespignani, A. *Evolution and Structure of the Internet: a Statistical Physics Approach* (Cambridge University Press, Cambridge, 2004).
- [7] Strogatz, S. H. Complex systems: Romanesque networks. *Nature* **433**, 365-366 (2005).
- [8] Watts, D. J., Strogatz, S. H. Collective dynamics of ‘small-world’ networks. *Nature* **393**, 440-442 (1998).
- [9] Barabási, A.-L., Albert, R. Emergence of Scaling in Random Networks. *Science* **286**, 509-512 (1999).
- [10] Hartwell, L. H., Hopfield, L. H., Leibler, S., Murray, A. W. From molecular to modular cell biology. *Nature* **402**, C47-C52 (1999).
- [11] Ravasz, E., Somera, A. L., Mongru, D. A., Oltvai, Z. N., Barabasi, A.-L. Hierarchical Organization of Modularity in Metabolic Networks. *Science* **297**, 1551-1555 (2002).
- [12] Girvan, M., Newman, M. E. J. Community structure in social and biological networks. *Proc. Natl. Acad. Sci.* **99**, 7821-7826 (2002).
- [13] Palla, G., Derenyi, I., Farkas, I., Vicsek, T. Uncovering the overlapping community structure of complex networks in nature and society. *Nature* **435**, 814-818 (2005).
- [14] Erdős, P., Rényi, A. On the evolution of random graphs. *Publ. Math. Inst. Hung. Acad. Sci.* **5**, 17-61 (1960).
- [15] Albert, R., Jeong, H., Barabási, A.-L. Error and attack tolerance of complex networks. *Nature* **406**, 378-382 (2000).
- [16] Cohen, R., Erez, K., ben-Avraham, D., Havlin, S. Resilience of the Internet to Random Breakdowns. *Phys. Rev. Lett.* **85**, 4626-4628 (2000).

- [17] Newman, M. E. J. Assortative Mixing in Networks. *Phys. Rev. Lett.* **89**, 208701 (2002).
- [18] Song, C., Makse, H. A. Emergence of functional classes in the evolution of the yeast protein-protein interaction network. *preprint*.
- [19] Maslov, S., Sneppen, K. Specificity and Stability in Topology of Protein Networks. *Science* **296**, 910-913 (2002).
- [20] Pastor-Satorras, R., Vázquez, A., Vespignani, A. Dynamical and Correlation Properties of the Internet. *Phys. Rev. Lett.* **87**, 258701 (2001).
- [21] Albert, R., Jeong, H., Barabási, A.-L. Internet: Diameter of the World-Wide Web. *Nature* **401**, 130-131 (1999). <http://www.nd.edu/~networks>
- [22] Jeong, H., Tombor, B., Albert, R., Oltvai, Z. N., Barabási, A.-L. The large-scale organization of metabolic networks. *Nature* **407**, 651-654 (2000).
- [23] Burch, H., Cheswick, W. Mapping the Internet. *IEEE Computer* **32**, 97-98 (1999). <http://research.lumeta.com/ches/map>
- [24] van Kampen, N. G. *Stochastic Processes in Physics and Chemistry* (North Holland, Amsterdam, 1981).
- [25] *Database of Interacting Proteins* (DIP). <http://dip.doe-mbi.ucla.edu>
- [26] Kitano, H. Systems Biology: A Brief Overview. *Science* **295**, 1662-1664 (2002).
- [27] Dorogovtsev, S. N., Goltsev, A. V., Mendes, J. F. F. Pseudofractal scale-free web. *Phys. Rev. E* **65**, 066122 (2002).
- [28] Jung, S., Kim, S., Kahng, B. Geometric fractal growth model for scale-free networks. *Phys Rev E* **65**, 056101 (2002).
- [29] Li, L., Alderson, D., Tanaka, R., Doyle, J. C., Willinger, W. Towards a Theory of Scale-Free Graphs: Definition, Properties, and Implications. *Internet Mathematics* (2005). [cond-mat/0501169](http://arxiv.org/abs/cond-mat/0501169).

**Supplementary Information** accompanies the paper on [www.nature.com/naturephysics](http://www.nature.com/naturephysics)

**Correspondence** and requests for materials should be addressed to H. A. M ([makse@mailaps.org](mailto:makse@mailaps.org)).

**Acknowledgements.** We would like to thank J. Brujić for illuminating discussions and E. Ravasz for providing the data on the metabolic network. SH wishes to thank the Israel Science Foundation, ONR and Dysonet for support. This work is supported by the National Science Foundation, DMR-0239504 to HAM.

## SUPPLEMENTARY MATERIAL

The Supplementary Material section is organized as follows: Section I shows that the available scale-free models are non-fractals. Section II describes more results on the correlation supplementing the various analysis and calculations in the main text. Section III reveals that the statistical properties, in particular, the degree distribution keeps invariant under renormalization for real-world networks. Section IV explains in detail the various theoretical results presented in the main text and elaborates on the extensions of the minimal model of fractal growth. Finally, Section VI gives more details of the study of the robustness of fractal and non-fractal networks under intentional attack.

### I. STUDY OF SCALE-FREE MODELS

While the origin of the scale-free property can be reduced to two basic mechanisms: growth and preferential attachment, as exemplified by the Barabási-Albert model (BA model [9]), the empirical result of fractality cannot be explained only in those terms. Notice that the term "scale-free" coined by Barabási-Albert [9] refers to the absence of a typical number of links, as exemplified by a power-law distribution of degree connectivity, but it does not refer to the length scale invariance found in [4].

We find that all models of scale-free networks such as the BA model of preferential attachment [9], the hierarchical model [11], and the so-called pseudo fractal models and trees [27, 28] are non-fractals. In Fig. 5 we plot the number of boxes  $N_B$  versus  $\ell_B$  for the models showing that in all the cases the decay of  $N_B(\ell_B)$  is exponential or faster, indicating either an infinite  $d_B$  or not a well-defined fractal dimension.

In the present study we find the relation  $\gamma = 1 + \ln n / \ln s$ , by using  $d_B = \ln n / \ln a$ , and  $d_k = \ln s / \ln a$ , as explained in the text. However, non-fractal networks satisfy this relation as well despite the infinite fractal dimension  $d_B \rightarrow \infty$ . Thus in general we say that when  $\gamma = 1 + \ln n / \ln s$  is satisfied, then the degree distribution is invariant under renormalization.

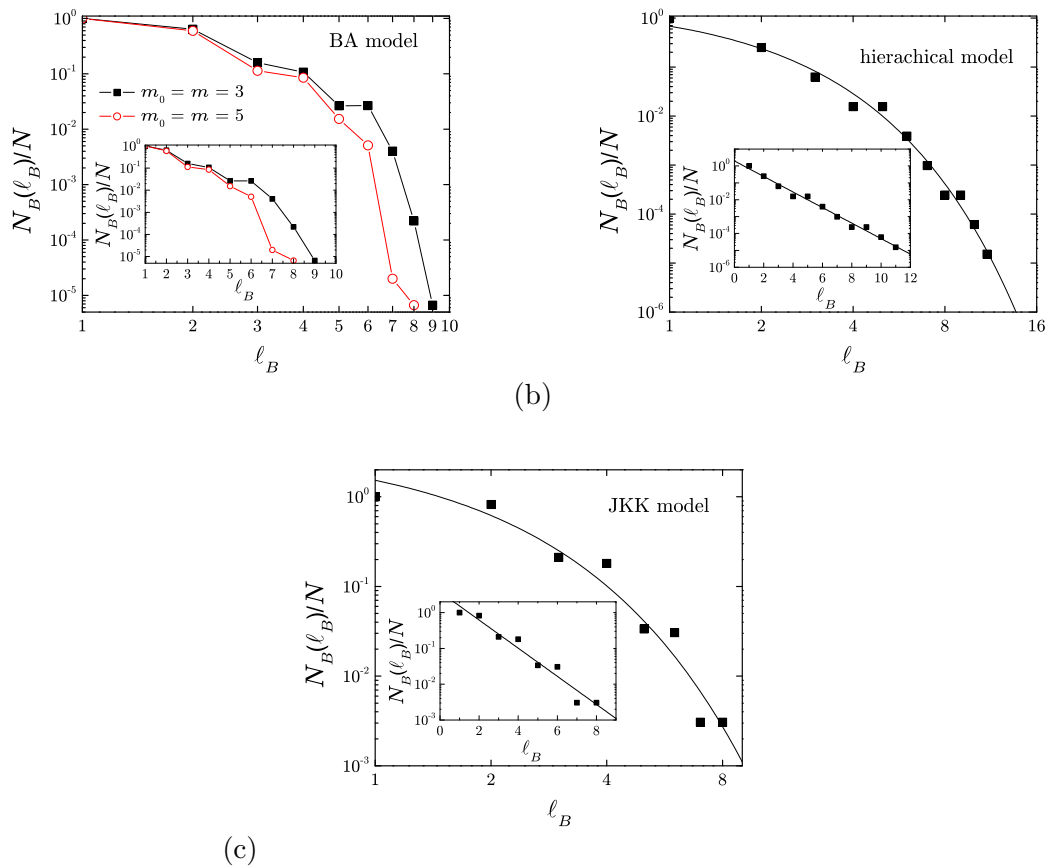


FIG. 5: Test of fractality in scale-free models. Number of boxes versus size of the boxes of different models showing that they do not follow a power-law, but an exponential (or faster) function as shown in the insets. Thus, they are non-fractal. (a) The BA model of preferential attachment [9], (b) the hierarchical model [11] and (c) the model of Jung, Kim, and Kahng (JKK model)[28] which is an example of pseudo fractal models as discussed by Dorogovtsev and Mendes [27].

## II. THE RANDOM UNCORRELATED SCALE-FREE MODEL AND THE CORRELATION PROFILES

It is instructive to analyze the degree of correlation in networks considering the deviations of the joint probability distribution  $P(k_1, k_2)$  from the random uncorrelated scale-free case  $P_r(k_1, k_2)$ . This latter model is obtained by, for instance, random swapping of the links in a given network [19], so that the degree distribution is preserved, but the correlation is completely lost.

The study of the ratio  $R(k_1, k_2) = P(k_1, k_2)/P_r(k_1, k_2)$  reveals that most of the networks

such as metabolic and protein interaction networks, the Internet and WWW are anticorrelated in comparison with the uncorrelated random case. This is because, even though this model is uncorrelated, there is still an effective attraction between the hubs since there is a large probability to randomly connect two nodes with large degrees. Thus, a plot of the ratio  $R = P(k_1, k_2)/P_r(k_1, k_2)$  reveals that most of the real networks are anticorrelated in comparison with the uncorrelated model. Therefore this ratio does not allow to distinguish between fractal and non-fractal networks.

In search of uncovering the extent of anticorrelation that are needed to obtain fractals we study the ratios for different networks by using the WWW as a reference (the use of any other network as a reference would lead to the same conclusions). This is done in the main text in Figs. 2c and 2d and for the model in Fig. 3b. These plots should be interpreted as follows: For instance, in Fig. 2c, let us take a large degree  $k_1 = 100$  as an example. Then we see that the ratio  $R_{E.coli}(k_1, k_2)/R_{WWW}(k_1, k_2)$  has a maximum for  $k_2 \approx 5$  (red-yellow scale) for small  $k_2$  ( $k_2 < 10$ ), and a minimum (blue scale) for large  $k_2 > 10$ . This means that the metabolic network has less probability to have hub-hub connection (two nodes with large degree connected) than a hub-non hub connection, when compared to the WWW. Therefore the metabolic network of E.coli is more anticorrelated than the WWW. In the same way, Fig. 2d shows that the hubs in the Internet have more probability to connect with other hubs than in the WWW, and therefore the Internet is less anticorrelated than the WWW. Therefore these patterns reveal that the fractal cellular networks are strongly anticorrelated (dissortative).

The same analysis is performed for the model in Fig. 3b in the main text. For instance, in this figure, given a large degree  $k_1 = 300$ , the ratio  $R_{e=1}(k_1, k_2)/R_{e=0.8}(k_1, k_2)$  is small (blue/green region) for small  $k_2$  ( $k_2 < 10$ ) but large (red/yellow region) for large  $k_2$  ( $k_2 > 10$ ). This means that the network with  $e = 1$  is more likely to have hub-hub connections than the  $e = 0.8$  case. Thus, the profile shows how  $e = 0.8$  is more anticorrelated than Mode I.

In summary, using a short notation, the strength of hubs repulsion satisfies: Uncorrelated scale-free model < Internet < WWW < protein interaction < metabolic networks. For the model we have: Mode I < Model with intermediate  $e$  < Mode II.

It is important to note that we can investigate the ratio between different networks such as  $R_{E.coli}(k_1, k_2)/R_{WWW}(k_1, k_2)$  because  $P(k_1, k_2)$  shows a power law behavior. Thus, even though the WWW and the metabolic network have different ranges of the values of  $k$ , power

law scaling of  $P(k_1, k_2)$  implies that the ratio is independent on the region of  $k_1$  and  $k_2$  used to plot this quantity.

### III. INVARIANCE OF DEGREE DISTRIBUTION

The renormalization procedure gives rise to a series of coarse-grained networks based on the box length  $\ell_B$ . The statistical properties of these networks, in particular, the degree distribution keeps invariant, as we showed in the previous work [4]. In this section, we verify this property again for a wide range of real-world networks including both fractal networks (WWW, protein interaction network of *yeast* and metabolic network of *E. coli*) and non-fractal networks (Internet), as we show in Fig. 6. It is important to note that even though the Internet is not fractal, the degree distribution is still invariant under renormalization.

### IV. THEORY

Here we elaborate on several theoretical expressions presented in the main text. We fully develop the theoretical framework of renormalization and its analogy with the time evolution of networks.

The multiplicative growth law is expressed as:

$$\begin{aligned}
 \tilde{L}(t+1) + L_0 &= a(\tilde{L}(t) + L_0), \\
 \tilde{N}(t+1) &= n\tilde{N}(t), \\
 \tilde{k}(t+1) &= s\tilde{k}(t), \\
 \tilde{n}_h(t+1) &= e\tilde{k}(t),
 \end{aligned}
 \tag{5}$$

where all the quantities have been previously defined in the main text. In Fig. 1a of the main text we provide an example of these quantities in a hypothetical growth process. In this example  $\tilde{N}(t) = 16$  nodes are renormalized with  $N_B(\ell_B) = 4$  boxes of size  $\ell_B = 3$  so that  $\tilde{N}(t-1) = 4$  nodes existed in the previous time step. The box size is defined as the maximum chemical distance in the box plus one. The chemical distance is the number of links of the minimum path between two nodes. The central box has a hub with  $k_{hub} = 8$  links, then  $\tilde{k}(t) = 8$ . After renormalization,  $k_B(\ell_B = 3) = 3$  for this central box, so that  $\tilde{k}(t-1) = 3$ . Out these three links, two are via a hub-hub connection (Mode I), thus  $n_h(\ell_B) = 2$  and  $\mathcal{E}(\ell_B) = 2/3$ , for this case.

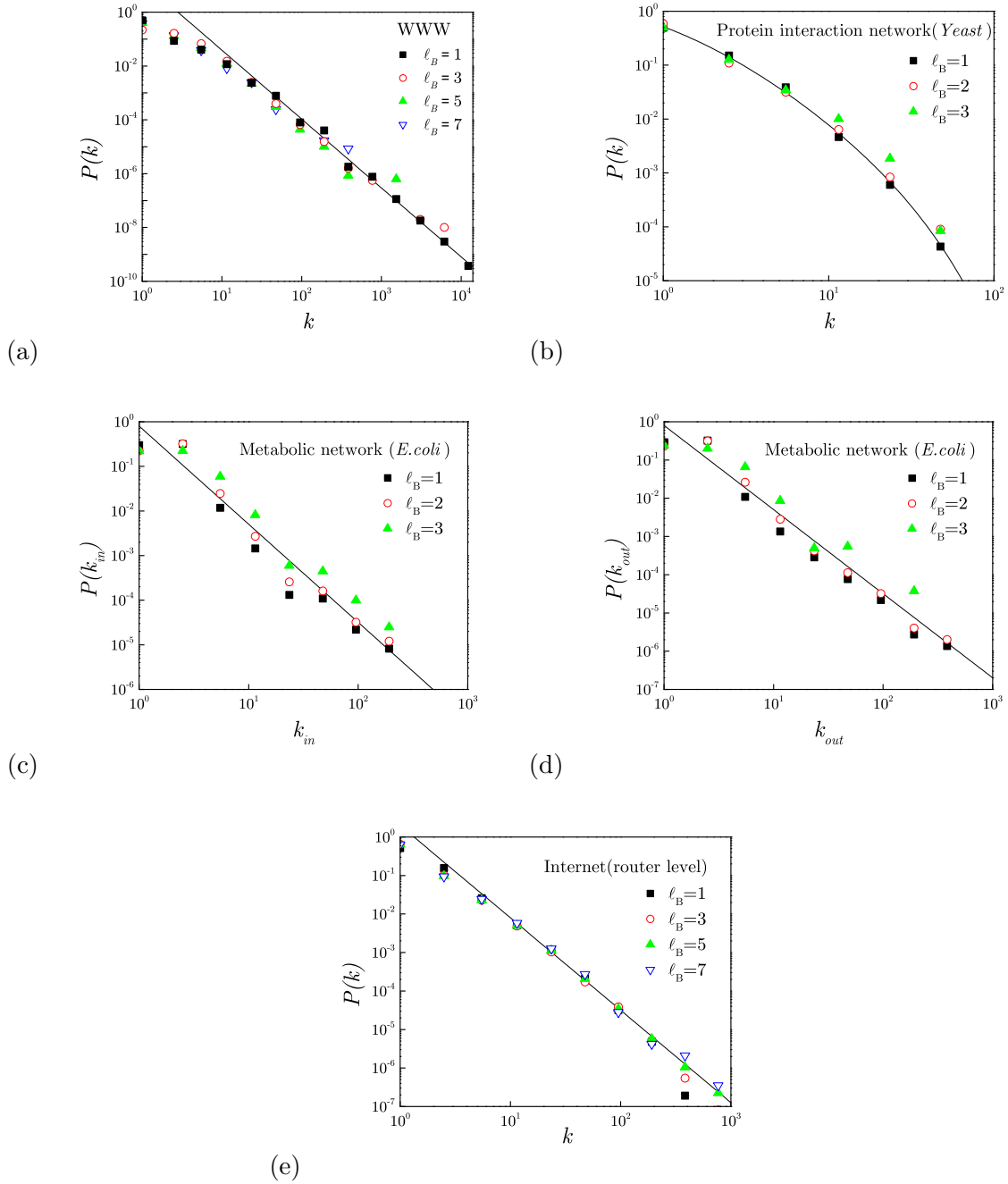


FIG. 6: Test of the invariance of degree distribution under renormalization. We plot the degree distribution of (a) WWW [21], (b) Protein interaction network of *yeast*, the inward degree (c) and the outward degree (d) of metabolic network of *E. coli* [22], and (e) Internet [23], according to different box size  $\ell_B$ .

TABLE I: Relation between time evolution and renormalization.

Quantity	Time evolution	Renormalization
diameter	$\tilde{L}(t_1) + L_0$	$L/(\ell_B + L_0)$
	$\tilde{L}(t_2) + L_0$	$L$
number of	$\tilde{N}(t_1)$	$N_B(\ell_B)$
nodes	$\tilde{N}(t_2)$	$N$
degree	$\tilde{k}(t_1)$	$k(\ell_B)$
	$\tilde{k}(t_2)$	$k_{hub}$
hub-hub	$\tilde{k}(t_1)$	$k(\ell_B)$
links	$\tilde{n}_h(t_2 t_1)$	$n_h(\ell_B)$

We obtain the relation between the quantities at two times  $t_2 > t_1$  as

$$\begin{aligned}
 \tilde{L}(t_2) + L_0 &= a^{t_2-t_1}(\tilde{L}(t_1) + L_0), \\
 \tilde{N}(t_2) &= n^{t_2-t_1}\tilde{N}(t_1), \\
 \tilde{k}(t_2) &= s^{t_2-t_1}\tilde{k}(t_1), \\
 \tilde{n}_h(t_2|t_1) &= e^{t_2-t_1}\tilde{k}(t_1).
 \end{aligned}
 \tag{6}$$

Notice that the quantity  $\tilde{n}_h(t_2|t_1)$  represents a special case. This quantity indicates the number of links at time  $t_2$ , which are connected to hubs generated before time  $t_1$ . To avoid the confusion with the other quantities, we introduce a new notation  $\tilde{n}_h(t_2|t_1)$  instead of  $\tilde{n}_h(t_2)$  as used for the other quantities in Eq. (6). We also notice that the notation  $\tilde{n}_h(t)$  in the main text Eq. (3) is then interpreted as  $\tilde{n}_h(t|t-1)$  for short. We then obtain:  $\tilde{n}_h(t_2|t_1) = e \tilde{n}_h(t_2-1|t_1) = \dots = e^{t_2-t_1} n_h(t_1|t_1) = e^{t_2-t_1} k(t_1)$ , where we have used that  $n_h(t_1|t_1) = k(t_1)$ .

The relationship between the quantities describing the time evolution and the renormal-

ization is shown in Table I. They are formalized as follows:

$$\begin{aligned}
\ell_B + L_0 &= (\tilde{L}(t_2) + L_0)/(\tilde{L}(t_1) + L_0) = a^{t_2-t_1} \\
\mathcal{N}(\ell_B) &\equiv N_B(\ell_B)/N = \tilde{N}(t_1)/\tilde{N}(t_2) = n^{t_1-t_2}, \\
\mathcal{S}(\ell_B) &\equiv k_B(\ell_B)/k_{hub} = \tilde{k}_B(t_1)/\tilde{k}_B(t_2) = s^{t_1-t_2}, \\
\mathcal{E}(\ell_B) &\equiv n_h(\ell_B)/k_B(\ell_B) = \tilde{n}_h(t_2|t_1)/\tilde{k}(t_1) = e^{t_2-t_1}.
\end{aligned} \tag{7}$$

Here we define the additional ratios,  $\mathcal{N}$  and  $\mathcal{S}$ . Replacing the time interval  $t_2 - t_1$  by  $\ln(\ell_B + L_0)/\ln a$ , as obtained from the first equation in (7), we obtain:

$$\begin{aligned}
\mathcal{N}(\ell_B) &= (\ell_B + L_0)^{-\ln n/\ln a}, \\
\mathcal{S}(\ell_B) &= (\ell_B + L_0)^{-\ln s/\ln a}, \\
\mathcal{E}(\ell_B) &= (\ell_B + L_0)^{-\ln(1/e)/\ln a},
\end{aligned} \tag{8}$$

or

$$\begin{aligned}
\mathcal{N}(\ell_B) &= (\ell_B + L_0)^{-d_B}, d_B \equiv \ln n/\ln a, \\
\mathcal{S}(\ell_B) &= (\ell_B + L_0)^{-d_k}, d_k \equiv \ln s/\ln a, \\
\mathcal{E}(\ell_B) &= (\ell_B + L_0)^{-d_e}, d_e \equiv \ln(1/e)/\ln a,
\end{aligned} \tag{9}$$

which correspond to the equations described in the main text. Notice that we have considered  $L_0 = 0$  in Eqs. (1) for simplicity. Equations (9) are more general and accommodate the case of non-fractal networks which are characterized by exponential functions:

$$\begin{aligned}
\mathcal{N}(\ell_B) &\sim \exp(-\ell_B/\ell_0), \\
\mathcal{S}(\ell_B) &\sim \exp(-\ell_B/\ell'_0).
\end{aligned} \tag{10}$$

These expressions arise from Eqs. (9) by taking the limit of  $d_B \rightarrow \infty$ ,  $d_k \rightarrow \infty$ , and  $L_0 \rightarrow \infty$  while  $L_0/d_B \rightarrow \ell_0$  and  $L_0/d_k \rightarrow \ell'_0$ , where  $\ell_0$  and  $\ell'_0$  are characteristic constants of the network.

### A. The minimal model

In the framework of the minimal model, we start with a star structure at  $t = 0$  as seen in Fig 7a. At each time step  $mk(t)$  new nodes are generated for each node with

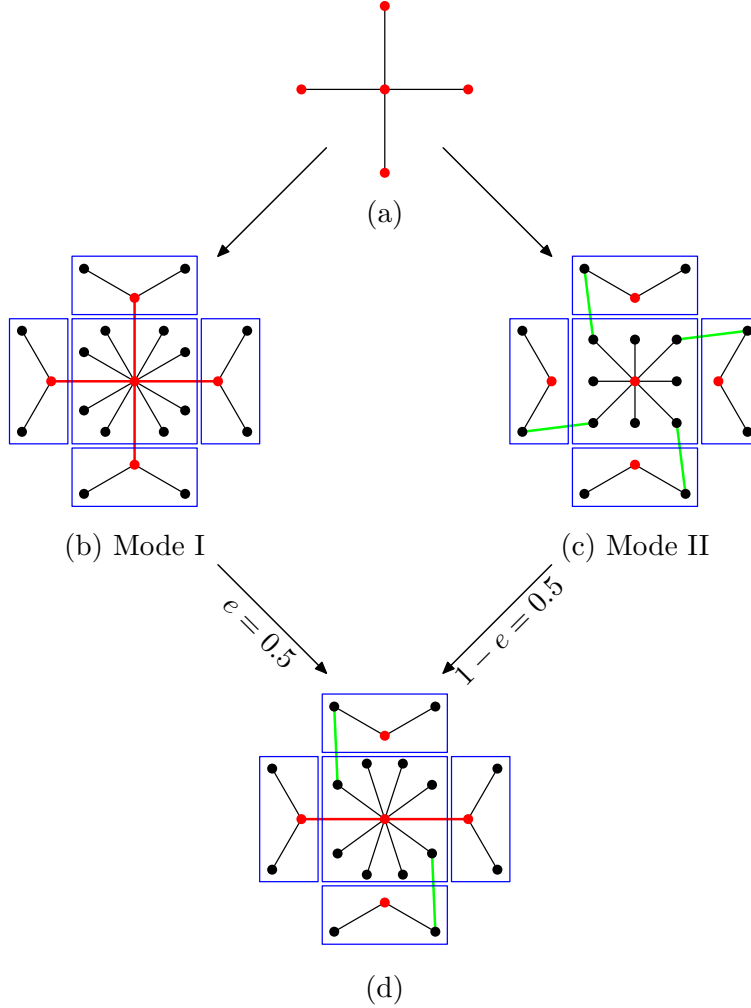


FIG. 7: Different modes of growth with  $m = 2$ . Starting with (a) five nodes at  $t = 0$ , the different connectivity modes lead to different topological structures, which are (b) Mode I, (c) Mode II and (d) combination of Mode I and II with probability  $e = 0.5$ .

degree  $k(t)$ , where  $m$  is an input parameter ( $m = 2$  in Fig. 7). Accordingly, we have  $\tilde{N}(t+1) = \tilde{N}(t) + 2m\tilde{K}(t)$ , where  $\tilde{K}(t)$  is the total number of links at time  $t$ . Since we do not consider the loop structure at the moment, we have  $\tilde{K}(t) = \tilde{N}(t)$ . Then we obtain  $\tilde{N}(t+1) = (2m+1)\tilde{N}(t)$ , or  $n = 2m+1$ . We find that the results of the model are independent on the initial configuration.

Then, two different connectivity modes are chosen as follows: Mode I, we keep all the old connections generated multiplicatively at time  $t$  (the red links in Fig. 7b). Mode II, all the old connections generated in the previous time time step are replaced by links between new generated nodes (see the green links in Fig. 7c).

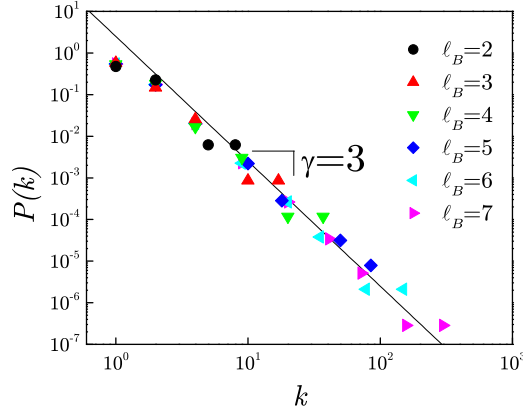


FIG. 8: Predictions of the model for  $e = 0.5$  for the degree distribution showing the power law behavior with  $\gamma = 3$  and its invariance under time evolution.

Mode I implies  $s = m + 1$ , since  $\tilde{k}(t + 1) = m\tilde{k}(t) + \tilde{k}(t)$ , where the term  $m\tilde{k}$  comes from newly generated nodes, and the term  $\tilde{k}$  comes from the links at previous time steps. The diameter of the network grows additively as:  $\tilde{L}(t + 1) = \tilde{L}(t) + 2$  ( $a = 1$ ,  $L_0 \rightarrow \infty$  and  $(a - 1)L_0 \rightarrow 2$  in Eqs. (5)) because at each step we generate one extra node at both sides of the network and therefore the size of the network is increase by 2, as seen in Fig. 7b. This implies  $\tilde{L}(t) \sim 2t$ . For this mode we obtain a non-fractal topology:  $N_B(\ell_B)/N \sim \exp(-\frac{\ln n}{2}\ell_B)$  and  $k(\ell_B)/k_{hub} \sim \exp(-\frac{\ln s}{2}\ell_B)$ ; a direct consequence of the linear growth of the diameter  $\tilde{L}(t)$  which implies that the network is small-world. Moreover,  $a = 1$  leads to  $d_B = \ln n / \ln a \rightarrow \infty$  in this case (non-fractal).

Mode II alone gives rise to a fractal topology but with a breakdown of the small-world property. The diameter increases multiplicatively  $\tilde{L}(t + 1) = 3\tilde{L}(t)$  ( $a = 3$  and  $L_0 = 0$  in Eqs. (5)), because we replace all the links at previous time step by the paths with chemical distance 3. The degrees grow as  $\tilde{k}(t + 1) = m\tilde{k}(t)$  according to our generation protocol, which leads to  $s = m$ . The multiplicative nature of  $\tilde{L}(t)$  leads to an exponential growth in the diameter with time,  $\tilde{L}(t) \sim e^{t \ln 3}$ , and consequently to a fractal topology with finite  $d_B$  and  $d_k$  according to Eqs. (7)-(8). This is seen because for this mode we have  $a = 3$ . We obtain  $N_B(\ell_B) \sim \ell_B^{-d_B}$  with finite  $d_B = \ln(2m + 1) / \ln 3$  and also  $k(\ell_B)/k_{hub} \sim \ell_B^{-d_k}$  with  $d_k = \ln m / \ln 3$ . However, the multiplicative growth of  $\tilde{L}$  leads to the disappearance of the small-world effect, which is replaced by a power-law dependence.

The general growth process is a stochastic combination of Mode I (with probability  $e$ ) and Mode II (with probability  $1-e$ , see Fig. 7d). We obtain  $\tilde{L}(t+1) = (3-2e)\tilde{L}(t)+2e$ , and  $a = 3 - 2e$  and  $L_0 = e/(1 - e)$ . Then, when  $e \rightarrow 1$  (Mode I)  $a = 1$  and  $d_B \rightarrow \infty$ ,  $L_0 \rightarrow \infty$  and we obtain a non-fractal topology. On the other hand, Mode II has  $e = 0$ , then  $L_0 = 0$  and  $a > 1$  and  $d_B$  is finite, following the fractal scaling. For an intermediate  $0 < e < 1$  this model predicts finite fractal exponents  $d_B$  and  $d_k$  and also predicts the small-world effect due to the presence of Mode I, as shown in the main text. This is seen in the exponential behavior of  $\langle M_c \rangle$  versus  $\ell_B$ .

In Fig. 8 we show further evidence that this model reproduces the self-similar properties found in fractal networks by plotting  $P(k)$ . We find that the model is modular since  $P(k)$  is invariant under renormalization with  $\gamma = 1 + \ln n / \ln a = 3$ , which is in agreement with the empirical findings of Fig. 6. Consistent with our predictions we find that  $d_k = \ln s / \ln a = 3.3$ .

Finally we summarize the predictions of the model. The fractal dimension is  $d_B = \ln n / \ln a$ , and in the framework of the minimal model with probability  $e$ , we find  $a = 3 - 2e$  and  $L_0 = e/(1 - e)$ . Then, when  $e \rightarrow 1$  (Mode I)  $a = 1$  and  $d_B \rightarrow \infty$ ,  $L_0 \rightarrow \infty$  and  $\ell_0 = L_0/d_B = 2/\ln n$  giving a non-fractal topology as in Eqs. (10). On the other hand, Mode II has  $e = 0$ , then  $L_0 = 0$  and  $a > 1$  and  $d_B$  is finite, following the fractal scaling of Eqs. (9), as long as the growth of the number of nodes is multiplicative with a well-defined value of  $n$ . The fact that  $a = 1$  implies a linear growth of the diameter  $\tilde{L}(t) \sim 2t$ , which produces the small-world property. An intermediate model with, for instance  $e = 0.8$  gives rise to a fractal network with the small world effect, as shown by the scaling of  $N_B(\ell_B)$  in Fig. 3c and  $\mathcal{E}(\ell_B)$  in Fig. 3d, in the main text.

## B. Additional supporting evidence for the fractal network model

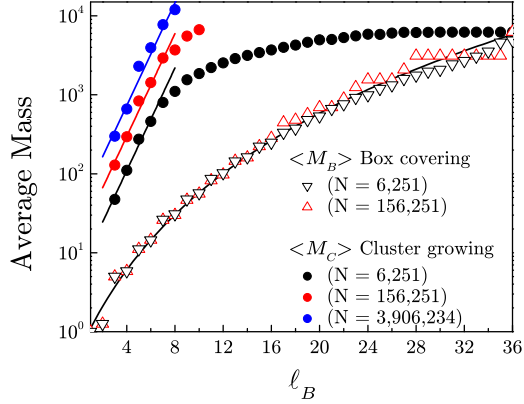
Evidence is given in Fig. 9a for the minimal model with parameter  $e = 0.8$ . We calculate (i) the mean number of nodes (mass) of the boxes tiling the network,  $\langle M_B(\ell_B) \rangle$  ( $\equiv N/N_B(\ell_B)$ ), by using the box covering methods, and (ii) the local mass  $\langle M_c(\ell_c) \rangle$  by averaging over boxes of size  $\ell_c$  around a randomly chosen node (the cluster growing method, see [2, 4]). The results show how the minimal model reproduces one of the main properties of fractal networks [4]: the power-law relation for the global average mass  $\langle M_B(\ell_B) \rangle \sim \ell_B^{d_B}$

with  $d_B = \ln 5 / \ln 1.4 = 4.8$  as a signature of fractality consistent with Eq. (1), and the exponential dependence of the local mass  $\langle M_c(\ell_c) \rangle \sim e^{\ell_c/\ell_0}$  as a signature of the small-world effect:  $\ell_c \sim \ln \langle M_c \rangle$ . Note that the cluster growing method is actually a way to measure the distance, while the box covering method measures the fractality [4]. The model leads also to a smooth monotonic scaling in the size distribution of modules as observed in [4]. The global small-world properties are treated next.

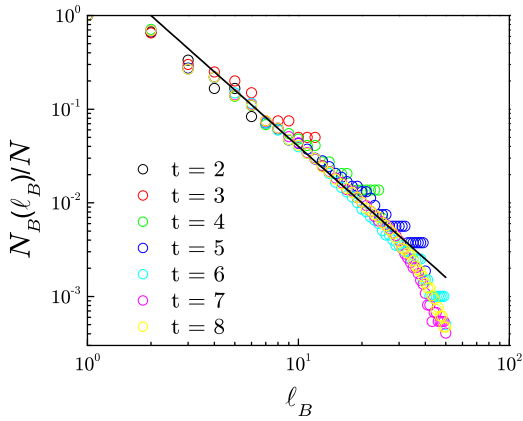
## V. GLOBAL SMALL WORLD: SHORT CUTS IN THE NETWORK

An important factor in the dynamics of real-world networks is the existence of randomness or noise in the growth process. The simplest type of noise is the appearance of random connections between nodes as exemplified in the Watts-Strogatz model of small world networks [8]. To investigate how noise affects the fractality of networks, we modify the dynamical law of the model as follows: at each time step,  $p\tilde{K}(t)$  number of links are added in at random, here  $\tilde{K}(t)$  is the total number of links at time  $t$ , and  $p$  is a constant that controls the fraction of noise. We build a fractal, small-world and scale-free topology with parameters  $m = 1.5$ ,  $e = 0.5$ , and add  $p = 1\%$  random connections at each time step. Our analytical considerations predict a box dimension  $d_B = 2$  in the absence of noise. The numerical simulation (see Fig. 9b) shows that this prediction of  $d_B$  still fits well to the simulated data, except for a small deviation at large box sizes, i.e. the added noise appears as an approximate exponential tail at large distances. Interestingly, this method could be used to test the appearance of noise in real complex networks, or to assess the quality of the data in, for instance, protein interaction networks obtained by yeast two-hybrid methods which are known to suffer from many false positives.

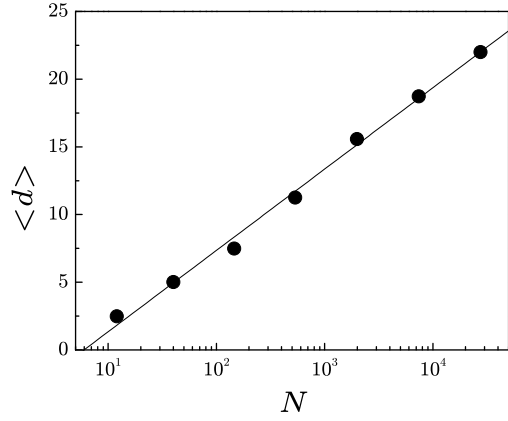
Most interestingly, the addition of noise leads to the small-world effect at the global level. In principle the existence of fractality seems to be at odds with the small-world effect. Fractality implies a power-law dependence on the distance, while the small-world effect implies an exponential dependence [4]. In Fig. 9a we show how the combination of Mode I and Mode II of growth leads to the global fractal property and the local small-world effect. In Fig. 9c we show that by adding a small fraction of short-cuts in a fractal complex network, we reproduce also the small-world effect at the global level. Using the algorithm explained above we add noise to the system and we find that the average distance  $\langle d \rangle$



(a)



(b)



(c)

FIG. 9: Additional predictions of the renormalization growth mechanism of complex networks. (a) The hallmark of fractality [4] is predicted by the minimal mechanism: the global tiling of the network evidences the fractality in the power-law dependence of the mass of the boxes,  $\langle M_B \rangle$ , while the local average of the cluster growing method  $\langle M_C \rangle$ , evidences the small-world effect. We show simulations for  $e = 0.8$  and different network size. The scaling of  $\langle M_B \rangle$  does not show finite size effects. The initial exponential dependence range of  $\langle M_C \rangle$  increases as the size of the network increases. (b)  $N_B$  vs  $l_B$  for the model with  $e = 0.5$  shows that the fractality still holds in the presence of random noise. The straight line gives the theoretical prediction of the model  $d_B = 2$ . (c) Average of the shortest path between two nodes as a function of the system size showing the global small world for the model ( $e = 0.5$ ).

over all pairs of vertices is

$$\langle d \rangle \sim 2.61 \ln N, \quad (11)$$

(Fig. 9c), indicating that the fractal model also predicts the global small-world. We notice that the fraction of short cuts needed to obtain the global small-world is very small, around 1%.

## VI. RESILIENCE OF FRACTAL NETWORKS UNDER INTENTIONAL ATTACK

To compare the stability of fractal and non-fractal networks under intentional attack (by removing hubs one by one from the largest to the smallest one), we generate two networks with  $e = 0$  and  $e = 1$ . In general the threshold of collapse under attack depends on several parameters and not only on the correlated properties of the network. Since we wish to assess only the effects of anticorrelation for the vulnerability of the network, we set all the other parameters to be equal. Thus, we use the same  $N$ ,  $\langle k \rangle$ ,  $\gamma$ , and also the same number of loops in the structure. For this purpose we consider the number of intraloops inside the boxes and the number of interloops between boxes.

In practice, inside the box there are  $mk(t)$  newly generated nodes. We add  $ymk$  extra links between them to generate triangles ( $y$  is a given constant) to obtain loops inside the boxes. For this case, we can rewrite  $n = 2(1 + y)m + 1$ , and the clustering coefficient  $C(k) = (2ym/s)k^{-1}$ . Thus, this kind of loops give rise to the known scaling of the clustering coefficient with  $k$  [11].

Another type of loops appears when more than one link connects two boxes (interloops). We find empirically that these kind of loops are also arranged in a self-similar way and are characterized by a new scaling exponent. In the framework of the minimal model, this type of loops can be introduced by adding  $x$  number of links between boxes at each time step, instead of keeping one link between boxes. These links could be of type Mode II (i.e., links between non-hubs), or otherwise could be between a hub from one box to a non-hub in the other node. In fact, this last mode of growth is a third mode that can be considered in the minimal model. We have not included it so far for simplicity, since it does not give rise to any new result. In general this mode could be thought of as a modified Mode II, and does not change the general conclusions of this study.

Combining the loop structure inside the boxes (intraloops characterized by  $y$ ) and between boxes (interloops characterized by  $x$ ) we obtain a general formula for the average degree  $\langle k \rangle = 2(1 + y) + (x - 1)/m$ . In the case of the minimal tree structure discussed in the main text we have  $y = 0$  and  $x = 1$ , which leads to  $\langle k \rangle = 2$ , consistent with our previous arguments. These networks are then used to generate the structures used in the calculation of the vulnerability of networks under intentional attack, shown in Fig. 4.